Electronic Supporting Information

Highly efficient photocatalytic degradation over rose-like 1D/2D $La(OH)_3/(BiO)_2OHCl$ heterostructures boosted by rich oxygen vacancies and enhanced interfacial charge transfer

Ying Tan[a,‡], Qin Zhou[a,‡], Weiya Huang[a,*], Kangqiang Lu[a], Kai Yang[a], Xunjun Chen[a], Dan Li[b,*], Dionysios D. Dionysiou[c]

[a] *Faculty of Materials, Metallurgical and Chemistry, Jiangxi University of Science and Technology, Ganzhou 341000, P. R. China;*

[b] *College of Science, Health, Engineering and Education, Murdoch University, Murdoch 6150, Australia.*

[c] *Environmental Engineering and Science Program, Department of Chemical and Environmental Engineering, University of Cincinnati, Cincinnati, OH 45221-0012, USA*

[*] Corresponding authors:

E-mail address: hweiya@126.com (W.Y. Huang); L.Li@murdoch.edu.au (D. Li)

‡These authors contributed equally to this work.

Contents

Text S1. Materials

$Bi(NO_3)_3{\cdot}5H_2O$ (99%), $La(NO_3)_3{\cdot}6H_2O$ (99.9%) and $NH_3{\cdot}H_2O$ (25 - 28%) were purchased from Aladdin Industrial Corporation (Shanghai, China). Ethanol and KCl were purchased from Sinopharm Chemical Reagent Corporation (Shanghai, China). All chemicals and reagents were used without further purification.

Text S2. Characterization

The X-ray diffraction (XRD) spectra were recorded using the Bruker D8-Advance X-ray powder diffraction instrument with Cu Ka radiation (λ = 0.15418 nm). The morphology and surface composition structure were characterized by a scanning electron microscope (SEM, FEI Quanta 250) and a transmission electron microscope (TEM, FEI Tecnai G^2 20). The chemical compositions were analyzed by an X-ray photoelectron spectroscope (XPS, Thermo Scientific K-Alpha). The specific surface areas were measured by a nitrogen adsorption analyzer (Micromeritics ASAP 2020). The Fourier transform infrared (FT-IR) spectra were recorded on a Nicolet 5700 FT-IR spectrometer. The UV–Vis diffuse reflectance spectra (DRS) were recorded with a UV–Vis spectrophotometer (Shimadzu UV-2600) in the range of 200 – 800 nm. The electron spin resonance (ESR) spectra were recorded on an electron spin resonance spectrometer (Bruker A300) with 5,5-dimethyl-1-pyrroline N-oxide (DMPO: 50 mM, 0.2 mL). The surface photovoltage spectroscopy (SPV, Zhongjiao jinyuan, CEL-SPEC) was used to measure the photovoltaic response. The intermediate products of TC were analyzed by a high-performance liquid chromatograph-tandem mass spectrometer (HPLC-MS,

ThermoFisher Q-Exactive). The electrochemical measurements of samples were performed on an electrochemical workstation with a standard three-electrode system (Shanghai Chenhua, CHI 660D) and a 400-nm LED lamp (Silver Bead Technology, Zhenjiang, China) as the light source.

The concentrations of TC and o-NP in solutions were monitored by measuring their maximum absorbance on a UV–vis spectrophotometer (UV-8000, Shanghai Metsch Instrument Co., Ltd.), based on the maximum absorption wavelength of 357 nm or 270 nm, respectively. The removal efficiency can be obtained by using the Eq. (S1) [1]:

$$Removal\ efficiency = \left(1 - C/C_0\right) \times 100\% \quad \text{(S1)}$$

The photocatalytic degradation kinetics of TC and o-NP were further analyzed by using the pseudo-first-order reaction kinetic equation, shown as Eq. (S2) [2]:

$$ln\left(C/C_0\right) = -kt \quad \text{(S2)}$$

where C_0 and C is the initial and residual concentration (mg/L) of TC and o-NP in solution, respectively.

Total organic carbon contents (TOC) were tested by total organic carbon analyzer (vario-TOC). The TOC removal % can be obtained using the Eq. (S3):

$$TOC\ removal\ efficiency = (1 - TOC/TOC_0) \times 100\% \quad \text{(S3)}$$

where TOC_0 and TOC is initial and residual TOC in solution, respectively.

The time-resolved fluorescence emission decay spectra data were obtained using the steady state and transient state fluorescence spectrometer (Edinburgh UK, FLS980). The results were calculated by using the Eq. (S4) [3]:

$$\tau = \frac{A_1\tau_1^2 + A_2\tau_2^2 + A_3\tau_3^2}{A_1\tau_1 + A_2\tau_2 + A_3\tau_3} \quad \text{(S4)}$$

where τ is the average lifetime, τ_1~τ_3 is the respective decay lifetime, and A_1~A_3 is the corresponding weight factor.

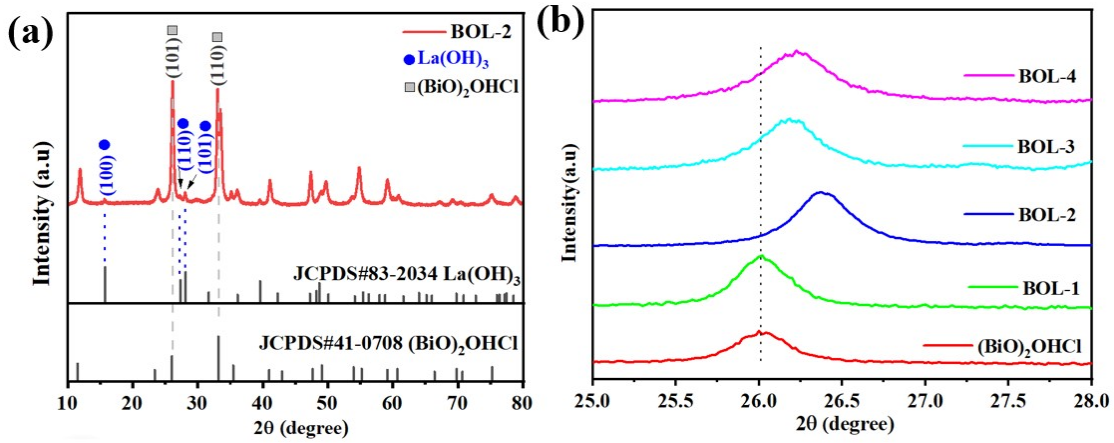

Fig. S1. (a) XRD pattern of BOL-2, (b) Magnified XRD patterns of catalysts at 2θ between 25° and 28°.

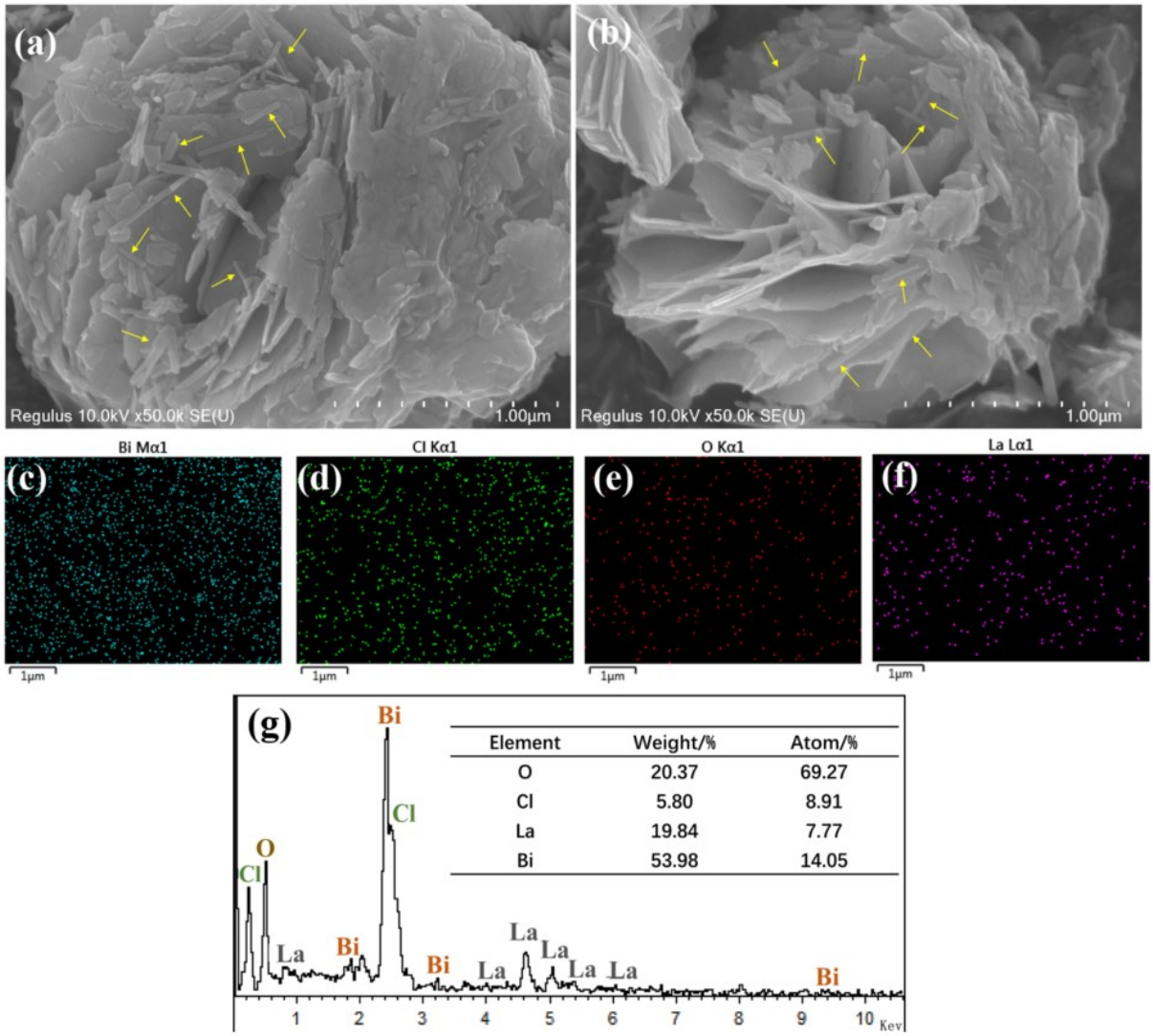

Fig. S2. (a, b) SEM images of two BOL-2 microflowers (the arrows point out the

growth of $La(OH)_3$ nanorods on $(BiO)_2OHCl$ nanosheets), (c-f) elemental mapping of BOL-2, (g) EDS analysis result of BOL-2.

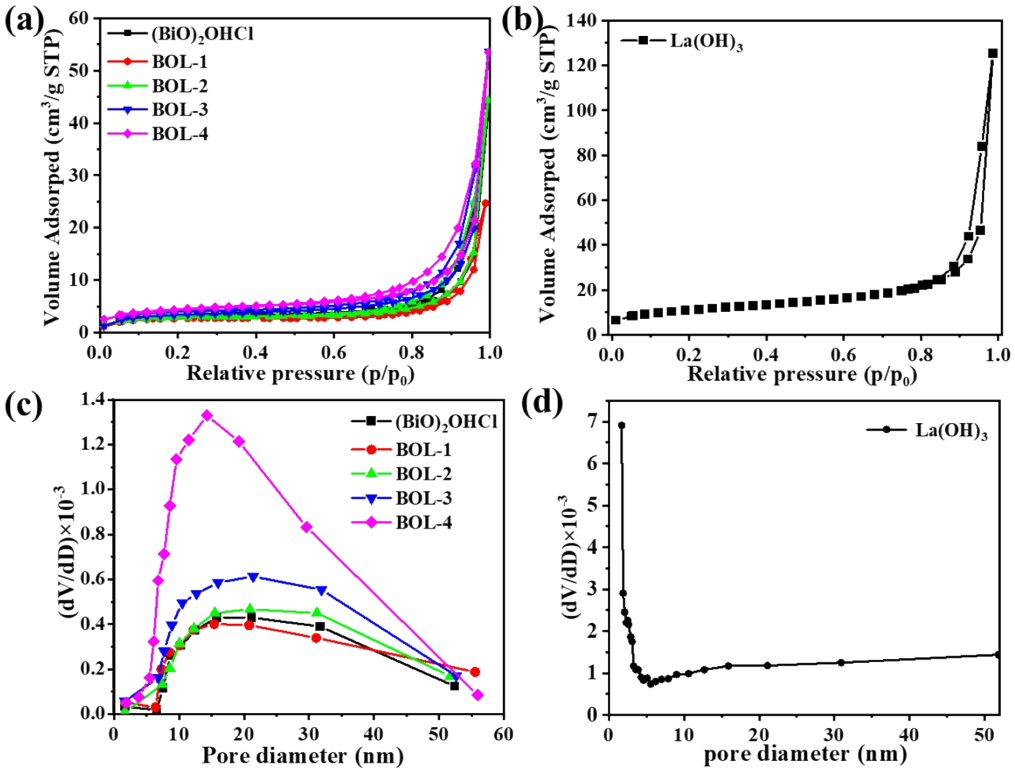

Fig. S3. N_2 adsorption-desorption isotherms of $(BiO)_2OHCl$ and BOL-x (x = 1, 2, 3 and 4) (a) and $La(OH)_3$ (b), Pore size distribution of $(BiO)_2OHCl$ and BOL-x (c) and $La(OH)_3$ (d).

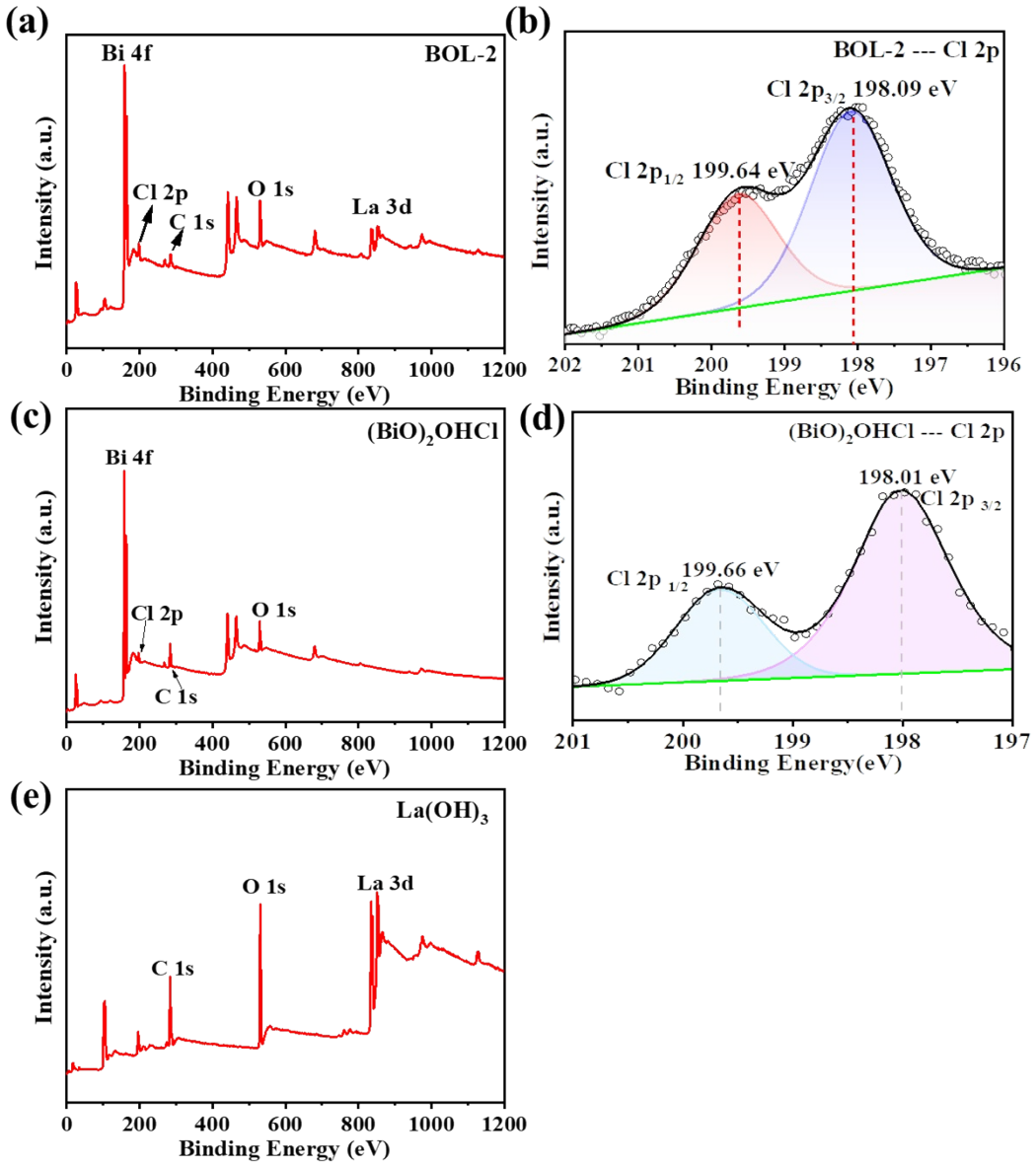

Fig. S4. (a) XPS survey spectrum and (b) high-resolution XPS spectrum of Cl 2p for BOL-2; (c) XPS survey spectrum and (d) high-resolution XPS spectrum of Cl 2p for $(BiO)_2OHCl$; (e)XPS survey spectrum for $La(OH)_3$.

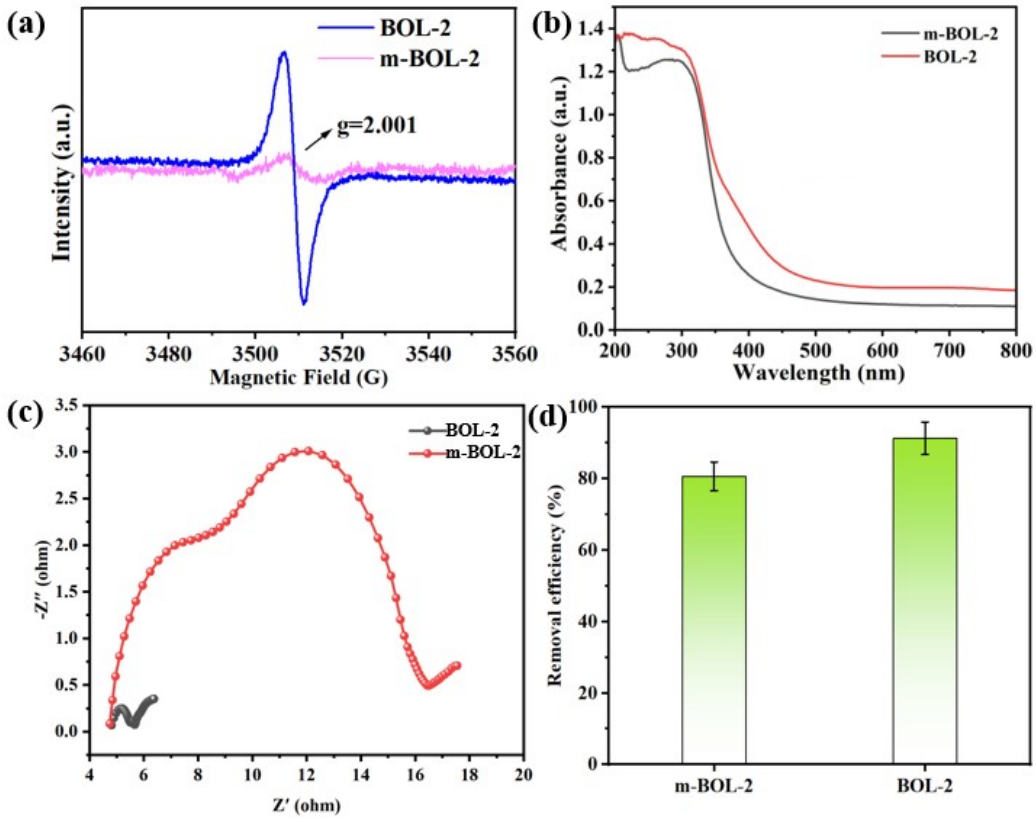

Fig. S5. (a) EPR spectra, (b) UV-Vis DRS, (c) EIS plots, (d) TC removal efficiencies of BOL-2 and m-BOL-2.

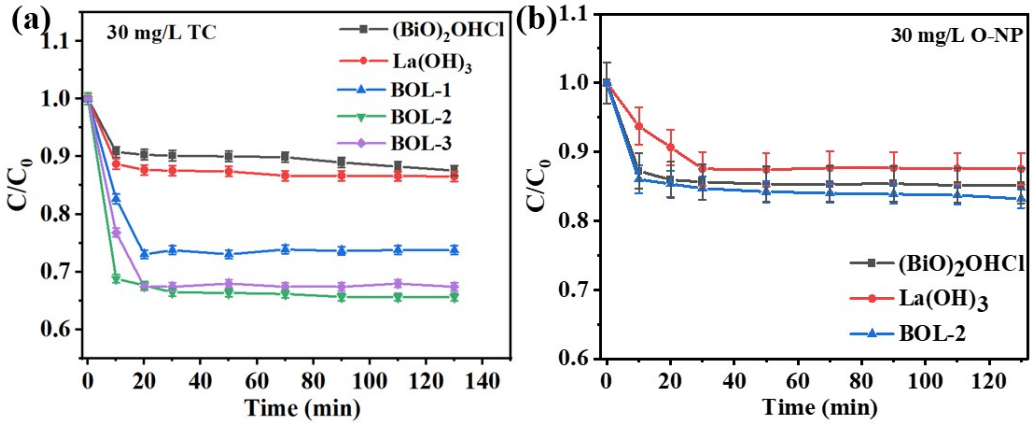

Fig. S6. TC (a) and o-NP (b) removal by adsorption in the dark.

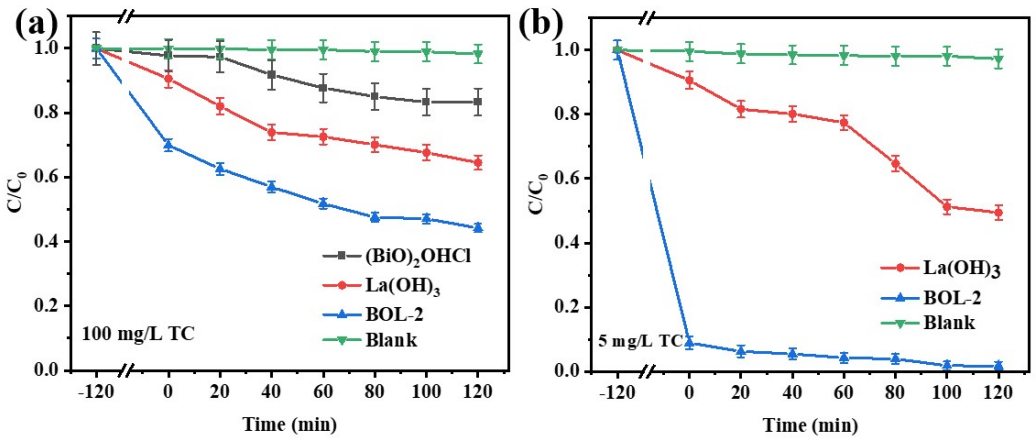

Fig. S7. TC removal, by adsorption in the dark and photocatalytic degradation under visible light, from the solution with (a) C_0 = 100 mg/L; (b) C_0 = 5 mg/L.

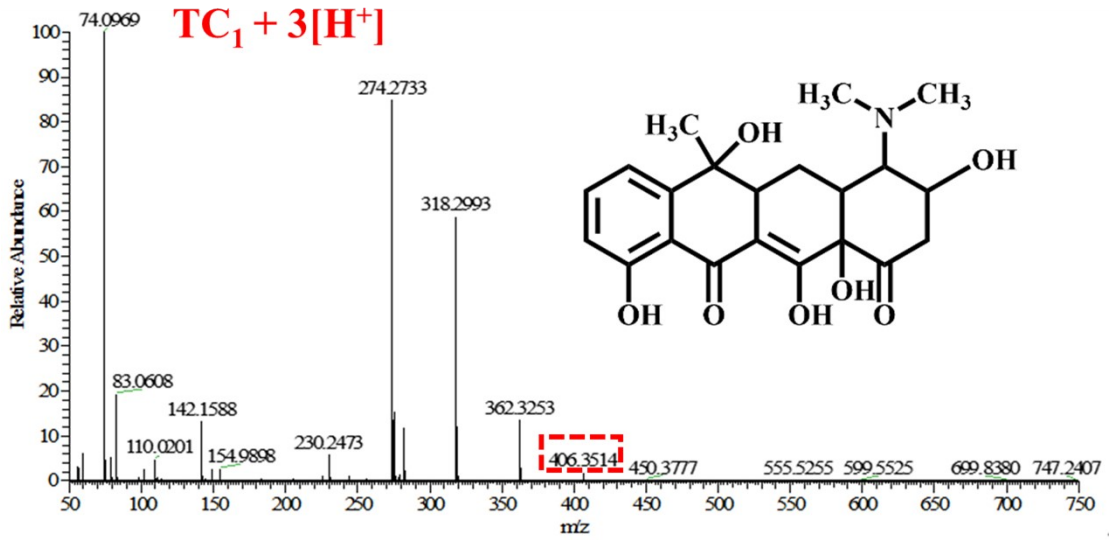
TC1 + 3[H+]
74.0969
274.2733
318.2993
83.0608
142.1588
362.3253
110.0201
154.9898
230.2473
406.3514
450.3777
555.5255
599.5525
699.8380
747.2407
Relative Abundance
m/z
H3C
CH3
N
OH
O

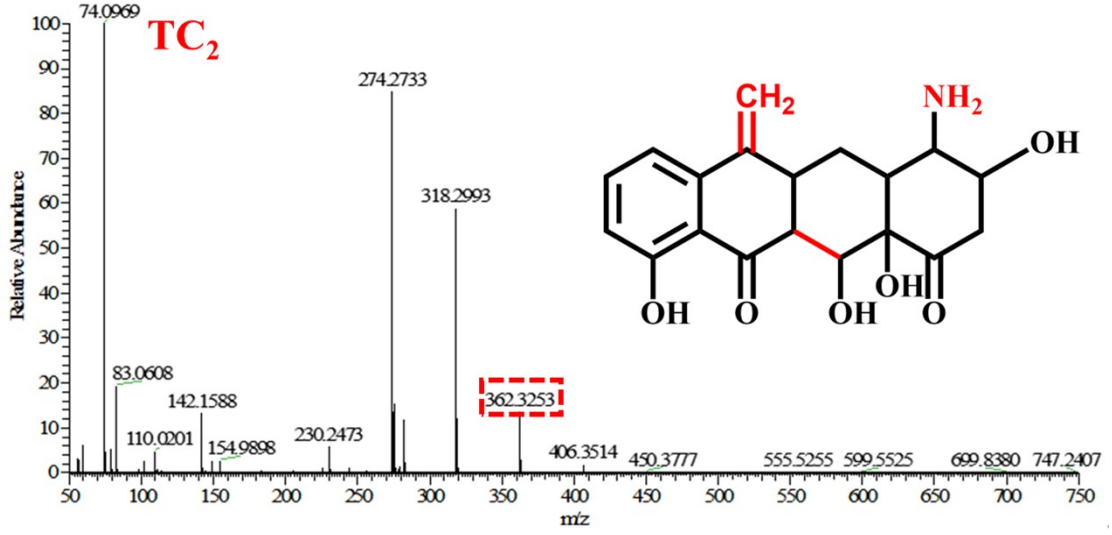
TC2
74.0969
274.2733
318.2993
83.0608
142.1588
362.3253
110.0201
154.9898
230.2473
406.3514
450.3777
555.5255
599.5525
699.8380
747.2407
Relative Abundance
m/z
CH2
NH2
OH
O

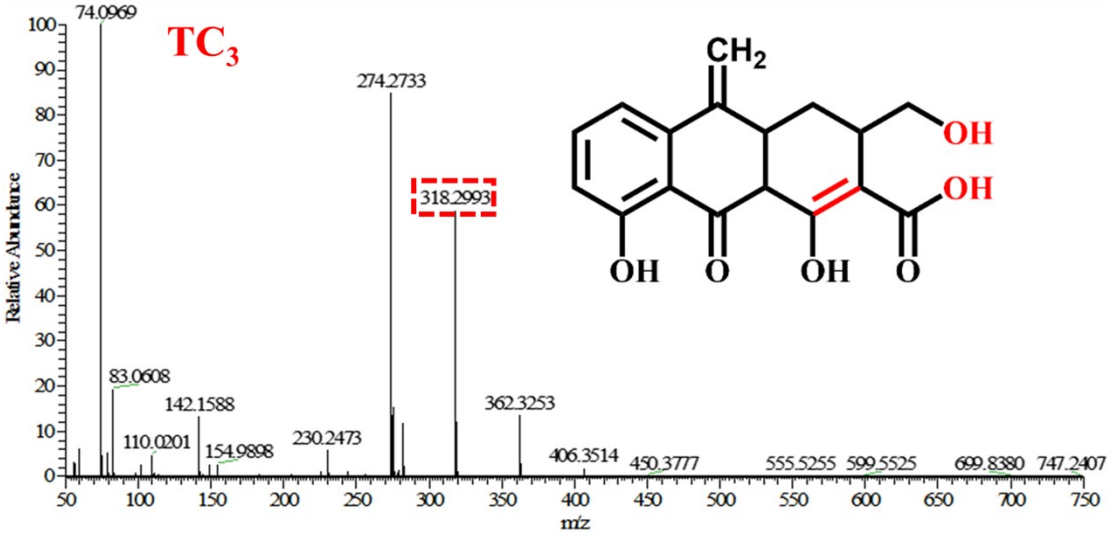
TC3
74.0969
274.2733
318.2993
83.0608
142.1588
362.3253
110.0201
154.9898
230.2473
406.3514
450.3777
555.5255
599.5525
699.8380
747.2407
Relative Abundance
m/z
CH2
OH
O

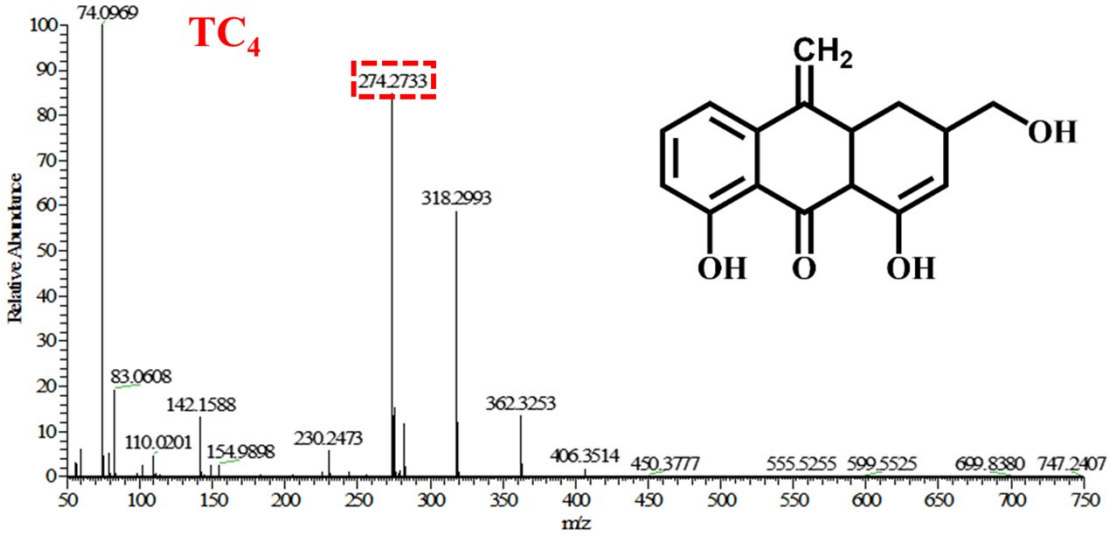
TC4
74.0969
274.2733
318.2993
83.0608
142.1588
110.0201
154.9898
230.2473
362.3253
406.3514
450.3777
555.5255
599.5525
699.8380
747.2407
Relative Abundance
m/z
CH2
OH
OH
O
OH

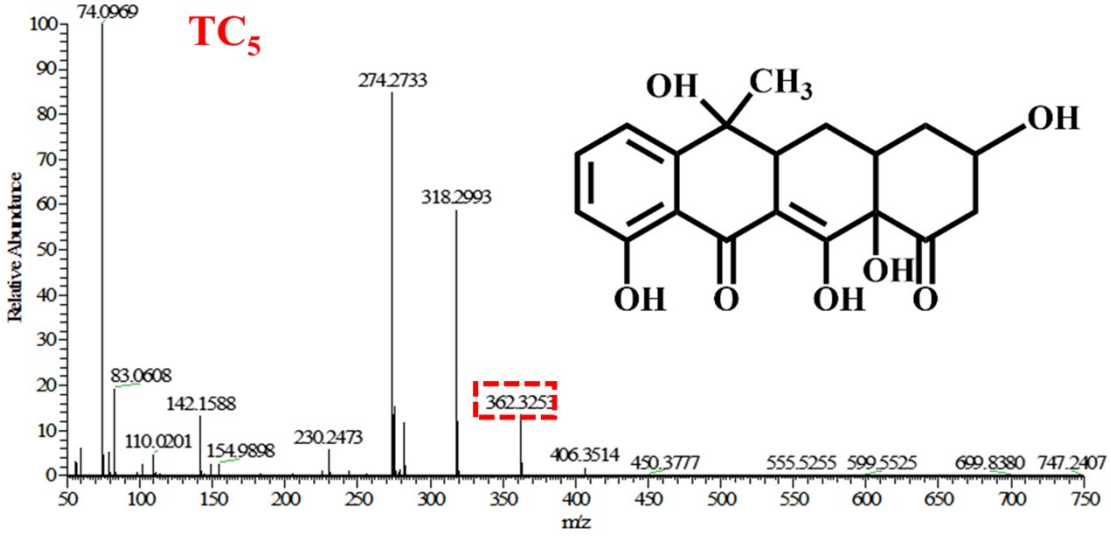
TC5
74.0969
274.2733
318.2993
83.0608
142.1588
110.0201
154.9898
230.2473
362.3253
406.3514
450.3777
555.5255
599.5525
699.8380
747.2407
Relative Abundance
m/z
OH
CH3
OH
OH
O
OH
OH
O

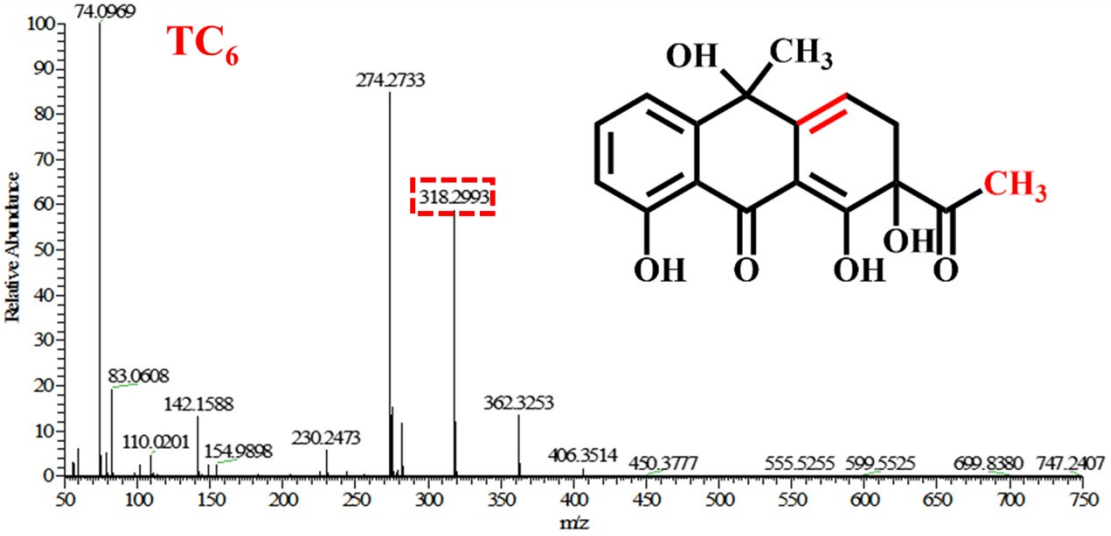
TC6
74.0969
274.2733
318.2993
83.0608
142.1588
110.0201
154.9898
230.2473
362.3253
406.3514
450.3777
555.5255
599.5525
699.8380
747.2407
Relative Abundance
m/z
OH
CH3
CH3
OH
OH
O
OH
O

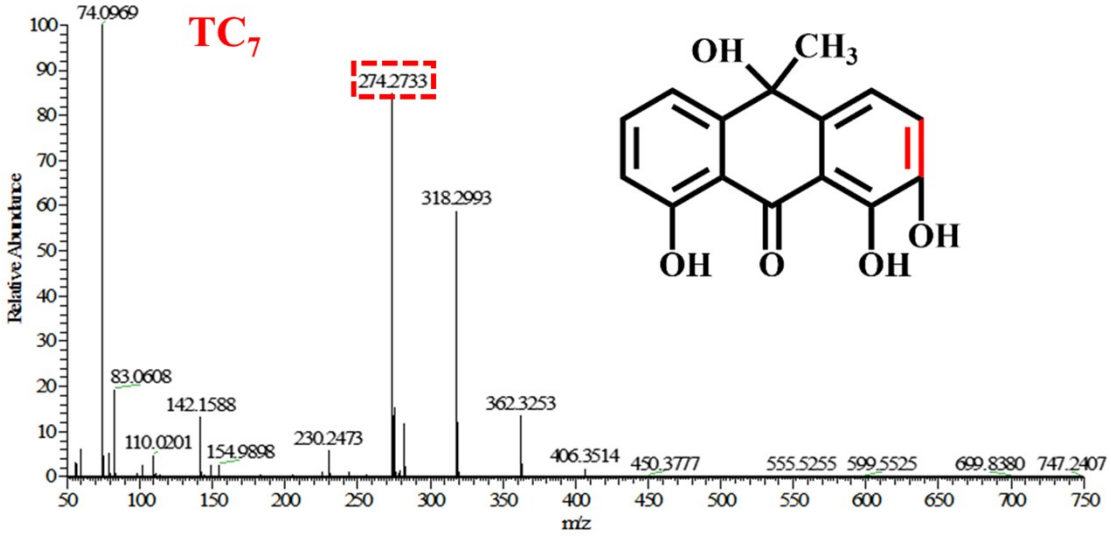
TC7
74.0969
274.2733
318.2993
83.0608
142.1588
110.0201
154.9898
230.2473
362.3253
406.3514
450.3777
555.5255
599.5525
699.8380
747.2407
Relative Abundance
m/z
OH
CH3
OH
O
OH
OH

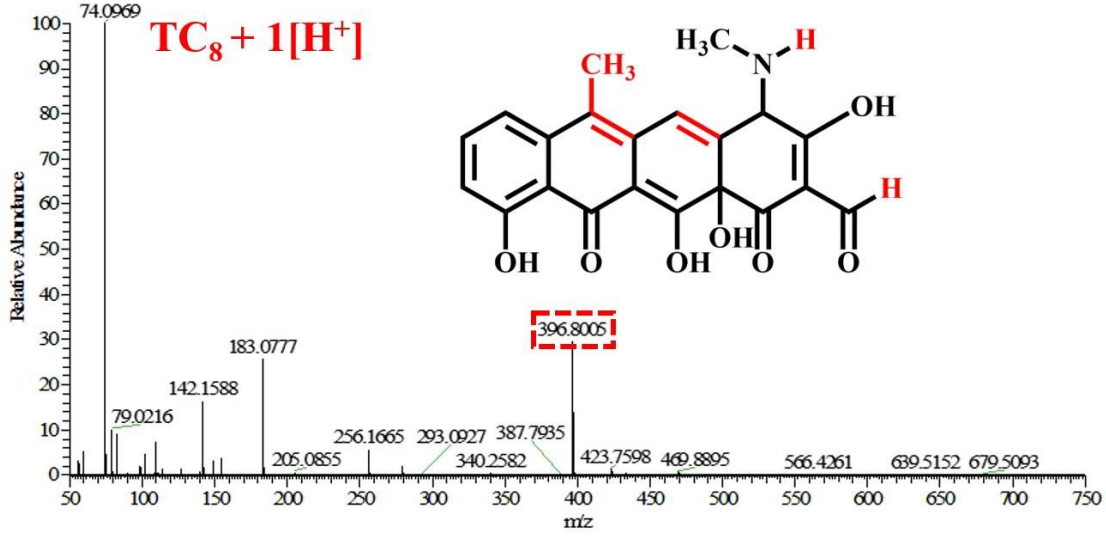
TC8 + 1[H+]
74.0969
396.8005
183.0777
142.1588
79.0216
256.1665
293.0927
387.7935
205.0855
340.2582
423.7598
469.8895
566.4261
639.5152
679.5093
Relative Abundance
m/z
H3C
N
H
CH3
OH
H
OH
OH
O
OH
O
O

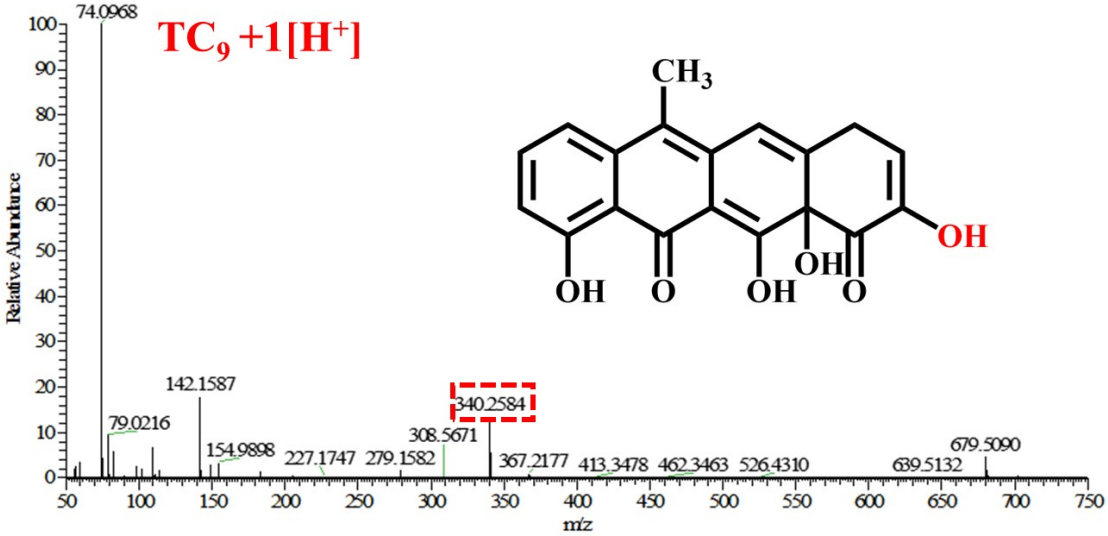
TC9 +1[H+]
74.0968
142.1587
340.2584
79.0216
154.9898
308.5671
227.1747
279.1582
367.2177
413.3478
462.3463
526.4310
639.5132
679.5090
Relative Abundance
m/z
CH3
OH
OH
OH
OH
O
OH
O

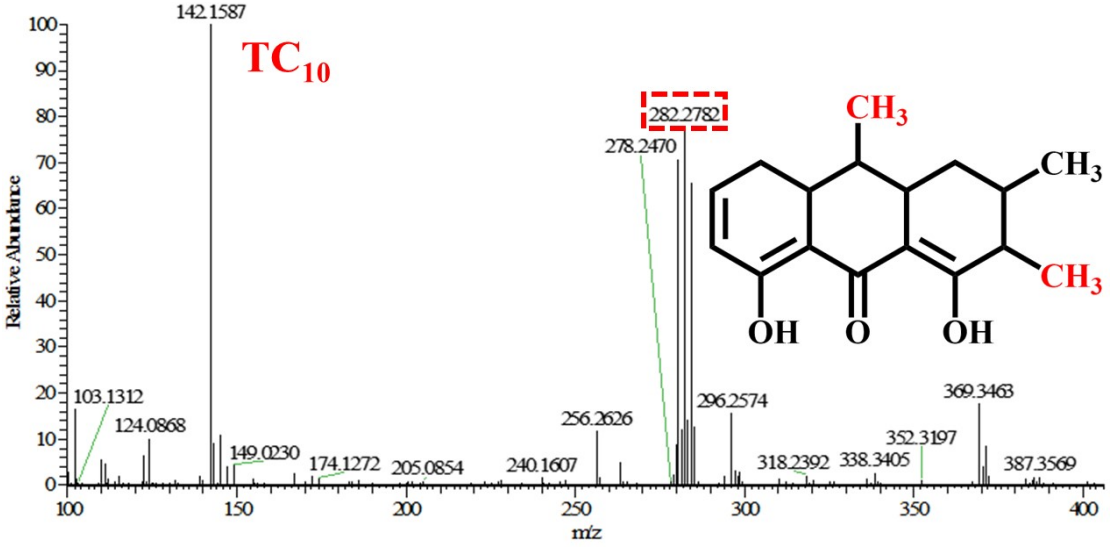
TC10
142.1587
282.2782
278.2470
CH3
CH3
CH3
OH
O
OH
103.1312
124.0868
149.0230
174.1272
205.0854
240.1607
256.2626
296.2574
318.2392
338.3405
352.3197
369.3463
387.3569
Relative Abundance
m/z

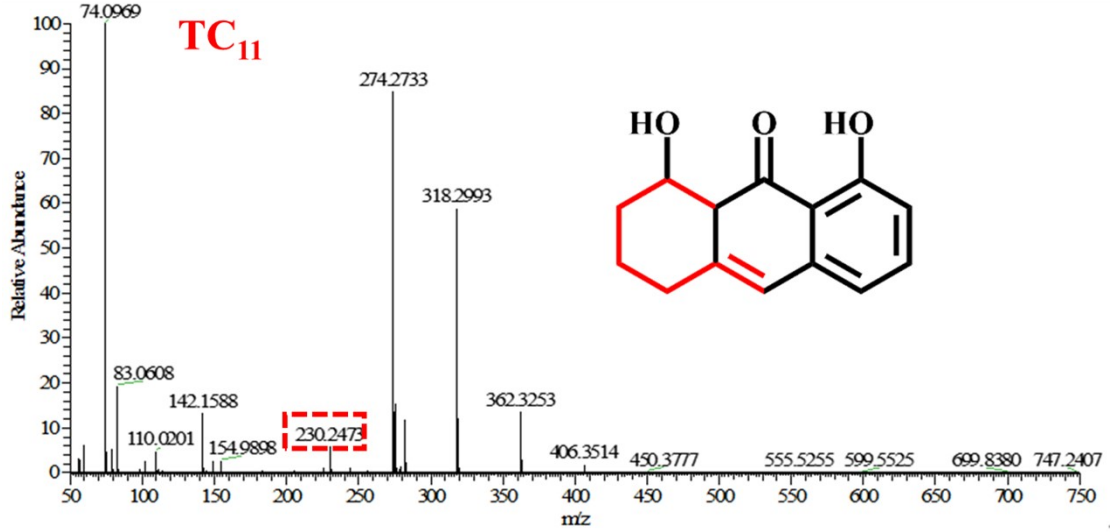
TC11
74.0969
274.2733
318.2993
HO
O
HO
83.0608
142.1588
110.0201
154.9898
230.2473
362.3253
406.3514
450.3777
555.5255
599.5525
699.8380
747.2407
Relative Abundance
m/z

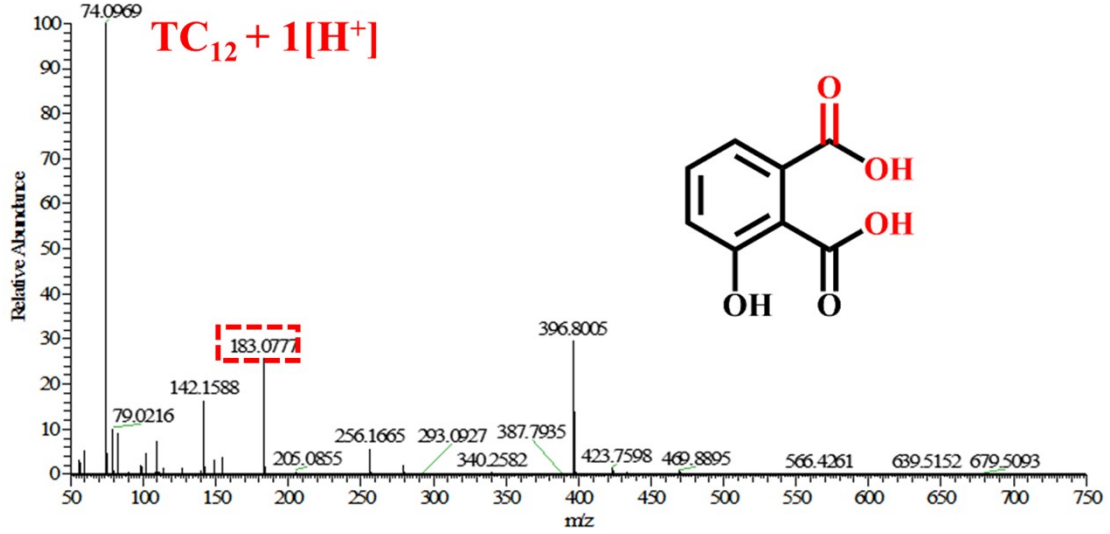
TC12 + 1[H+]
74.0969
O
OH
OH
OH
O
183.0771
396.8005
142.1588
79.0216
256.1665
293.0927
387.7935
205.0855
340.2582
423.7598
469.8895
566.4261
639.5152
679.5093
Relative Abundance
m/z

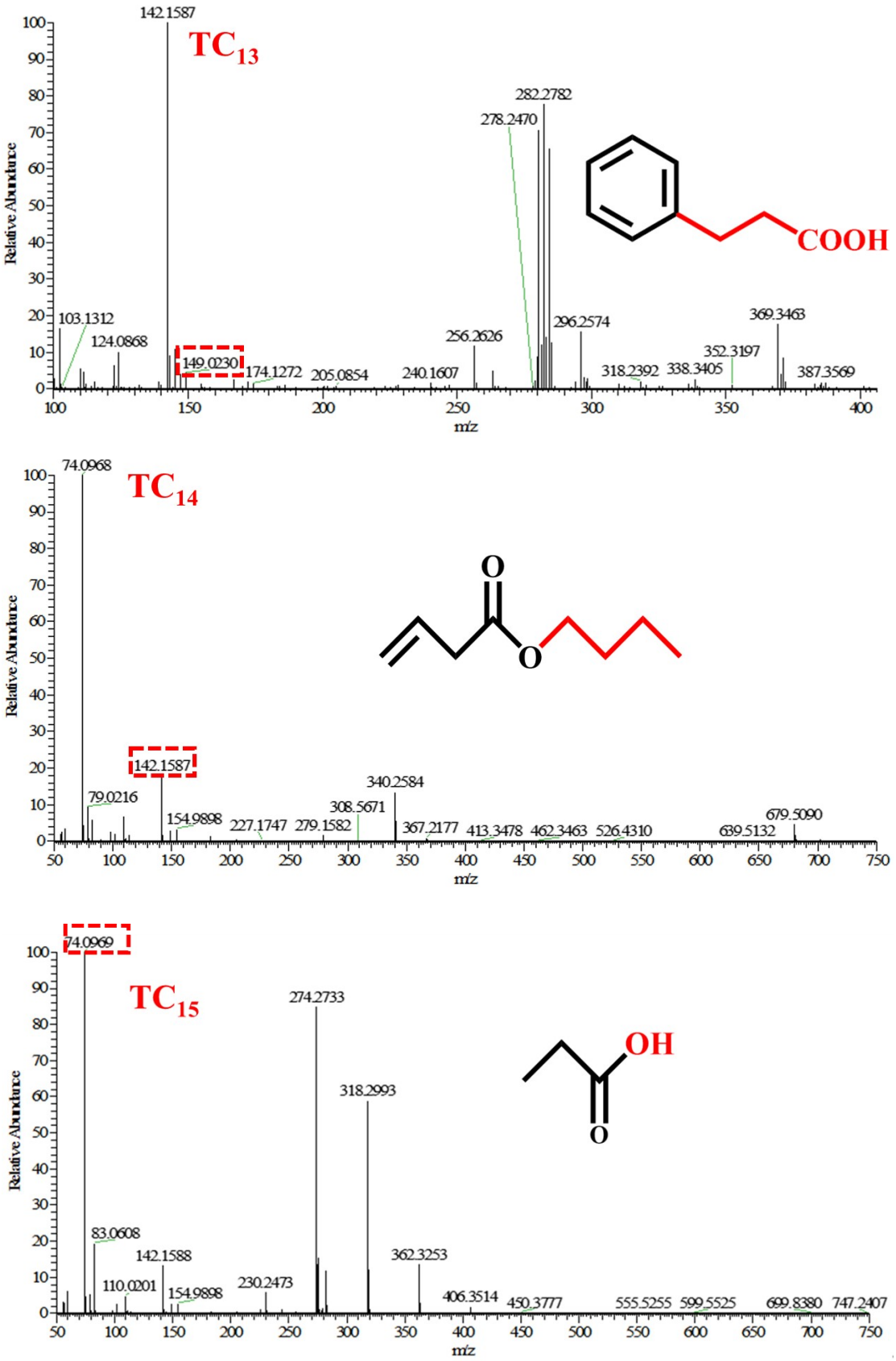

Fig. S8. HPLC-MS spectra of intermediates in the photocatalytic degradation of TC

using BOL-2.

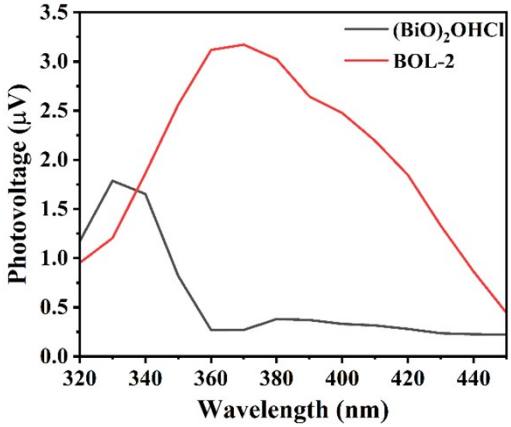

Fig. S9. Surface photovoltage (SPV) spectra of BOL-2 and $(BiO)_2OHCl$.

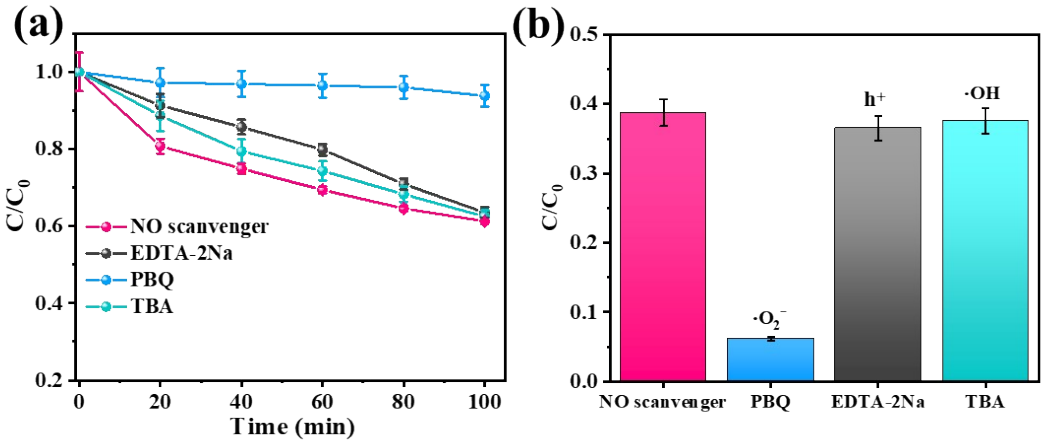

Fig. S10. Effect of different trapping agents on the photocatalytic degradation of TC by using pristine $(BiO)_2OHCl$ (a) over different periods of reaction time and (b) after 100 min reaction.

Table S1. Band gap values of $(BiO)_2OHCl$, $La(OH)_3$ and BOL-x (x = 1, 2, 3 and 4).

Sample	$(BiO)_2OHCl$	$La(OH)_3$	BOL-1	BOL-2	BOL-3	BOL-4
band gap value (eV)	3.04	2.95	2.18	2.51	2.92	3.12

Table S2. Information of antibiotic removal by BOL-2 and various bismuth-based catalysts from other studies.

Photocatalyst (dosage)	Light source	antibiotics	Concentration (mg/L)	Removal %	Reference
BOL-2 (50 mg/80 mL)	LED lamp (λ = 420 nm)	TC[a]	30 10 5	91.3% 96.7% 98.3%	This work
m-BOL-2 (50 mg/80 mL)	LED lamp (λ = 420 nm)	TC[a]	30	80.6%	This work
$La(OH)_3/BiOCl$ (25 mg/50 mL)	LED light (λ ≥ 420 nm, 5 W)	TC[a]	20	85.0%	[4]
$La(OH)_3/BaTiO_3$ (100 mg/100 mL)	350 W Xe lamp	TC[a]	10	~100.0%	[5]
$Bi_2O_2(OH)_xCl_{2-x}$ (50 mg/100 mL)	LED lamp (λ ≥ 420 nm, 50 W)	CIP[b]	20	~90.0%	[6]
$(BiO)_2OHCl@Bi_{24}O_{31}Cl_{10}$ (10 mg/100 mL)	500 W metal halogen lamp (λ ≥ 420 nm)	LEV[c]	10	90.0%	[7]

[a]Tetracycline hydrochloride, [b]Ciprofloxacin, [c]levofloxacin

Table S3. Pseudo-first-order rate constants and correlation coefficients (R^2) for photocatalytic degradation of TC and o-NP over the as-prepared samples.

Sample	TC		o-NP	
	k (min^{-1})	R^2	k (min^{-1})	R^2
Blank	0.0001	0.9332	0.0001	0.9417
$(BiO)_2OHCl$	0.0048	0.9569	0.0037	0.9538
$La(OH)_3$	0.0063	0.9953	0.0094	0.9963
BOL-1	0.0087	0.9899	0.0061	0.9366
BOL-2	0.0169	0.9670	0.0235	0.9560
BOL-3	0.0100	0.9978	0.0168	0.9612
BOL-4	0.0075	0.9872	0.0107	0.9962

Table S4. Charge carrier lifetime parameters of $(BiO)_2OHCl$ and BOL-2.

Sample	τ_1	τ_2	τ_3	A_1	A_2	A_3	τ/ns
$(BiO)_2OHCl$	1.9174	1.9173	1.9172	68.261	67.962	67.033	1.9173
BOL-2	2.2512	2.2511	2.2510	74.088	74.636	72.287	2.2511
$La(OH)_3$	0.9437	0.9436	0.9436	76.213	76.322	70.397	0.9436

References

[1] J. A. Jonidi, B K.akavandi, N. Jaafarzadeh, K. R. Rezaei, Ahmadi M, Akbar Babaei A. Fenton-like catalytic oxidation of tetracycline by AC@Fe_3O_4 as a heterogeneous persulfate activator: Adsorption and degradation studies, *J. Ind. Eng. Chem*., 2017, **45**, 323-333.

[2] C. Xu, Q.Zhou, W.Y. Huang, K. Yang, Y. C. Zhang, T.X. Liang, Constructing Z-scheme β-Bi_2O_3/ZrO_2 heterojunctions with 3D mesoporous SiO_2 nanospheres for efficient antibiotic remediation via synergistic adsorption and photocatalysis, *Rare Metals*., 2022, **41**, 2094-2107.

[3] D. Xiang, X .Hao, Z. Jin. Cu/CdS/MnOx Nanostructure-Based Photocatalyst for Photocatalytic Hydrogen Evolution, *ACS Appl. Nano Mater*., 2021, 4, 13848-13860.

[4] Z. Zhou, H. Xu, D. Li, Z. Zou, D. Xia. Microwave-assisted synthesis of $La(OH)_3$/BiOCl n-n heterojunctions with high oxygen vacancies and its enhanced photocatalytic properties, *Chem. Phys. Lett*., 2019, **736**, 136805.

[5] B.Wang, K. Wei, F. Chen, Y. Wang, G. He, W. Li, J. Liu, Q. He. Effects of active species on degrading A-ring of tetracycline in the Z-scheme heterostructured core-shell $La(OH)_3$@$BaTiO_3$ composition, *J. Alloys Compd.*, 2019, **804**, 100-110.

[6] X. Wu, K. Li, Y. Li, G. Zhang, Motivating visible light photocatalytic activity of ultrathin $Bi_2O_2(OH)_xCl_{2-x}$ solid solution with exposed {001} facets by the co-effect of oxygen vacancy and OH replacement, *Nanoscale*., 2018, **10**, 15294-15302.

[7] C. Sun, R. Li, Y. Zhao, R. Yang, H. Xu, Ammonia-dependent synthesis of $(BiO)_2OHCl$@$Bi_{24}O_{31}Cl_{10}$ heterostructures with enhanced visible-light induced photocatalytic activities on levofloxacin removal, *J. Alloys Compd.*, 2022, **901**, 163647.